The IPEx Autonomy Test-Site: Terrestrial Testing of Autonomous Excavation in Lunar South Pole Conditions

Joseph M. Cloud
NASA Kennedy Space Center
KSC, FL, 32899, USA
NE-L6
joseph.m.cloud@nasa.gov

Andrew J. Nick
NASA Kennedy Space Center
KSC, FL, 32899, USA
UB-E
andrew.j.nick@nasa.gov

Bradley C. Buckles
NASA Kennedy Space Center
KSC, FL, 32899, USA
UB-E
bradley.buckles@nasa.gov

Kyle L. Dixon
NASA Kennedy Space Center
KSC, FL, 32899, USA
UB-G
kyle.l.dixon@nasa.gov

Thomas J. Muller
Bennett Aerospace
NASA Kennedy Space Center
KSC, FL, 32899, USA
thomas.j.muller@nasa.gov

Victoria V. Ortega
NASA Kennedy Space Center
KSC, FL, 32899, USA
UB-E
victoria.v.ortega@nasa.gov

Jonathan D. Smith
NASA Kennedy Space Center
KSC, FL, 32899, USA
UB-E
jonathan.d.smith@nasa.gov

Casey J. Clark
Astrion
NASA Kennedy Space Center
KSC, FL, 32899, USA
casey.j.clark@nasa.gov

Jeffrey E. Dyas
NASA Kennedy Space Center
KSC, FL, 32899, USA
NE-TE
jeffrey.e.dyas@nasa.gov

Elizabeth L. Zhang
NASA Kennedy Space Center
KSC, FL, 32899, USA
UB-E
elizabeth.l.zhang@nasa.gov

Kurt W. Leucht
NASA Kennedy Space Center
KSC, FL, 32899, USA
NE-XS
kurt.leucht@nasa.gov

Robert P. Mueller
NASA Kennedy Space Center
KSC, FL, 32899, USA
UB-E
rob.mueller@nasa.gov

Jason M. Schuler
NASA Kennedy Space Center
KSC, FL, 32899, USA
UB-E
jason.m.schuler@nasa.gov

***Abstract*— NASA's Artemis program aims to send humans to the lunar south pole (LSP), requiring in-situ resource utilization (ISRU) technologies like the ISRU Pilot Excavator (IPEx) to perform site preparation and resource extraction. The LSP is a uniquely challenging environment, characterized by low solar angles and long shadows that disrupt vision-based autonomy. To approximate these conditions, we developed the IPEx autonomy test-site, a 21.3×33.5 m enclosed area for testing excavation technologies under simulated LSP conditions. The test-site is equipped with granular material, scattered rocks, and a full-scale lander model. Strategically placed high-power lights replicate the low solar angles, while a motion capture system offers ground truth robot poses. Additional site awareness cameras provide complete coverage of the test area for monitoring. The test-site has been utilized to evaluate performance of both autonomous navigation and excavation tasks. Finally, we discuss initial results obtained from test runs, calculations compared against a digital simulation, features of the terrain that mimic the visual properties of lunar regolith, and challenges observed.**

TABLE OF CONTENTS

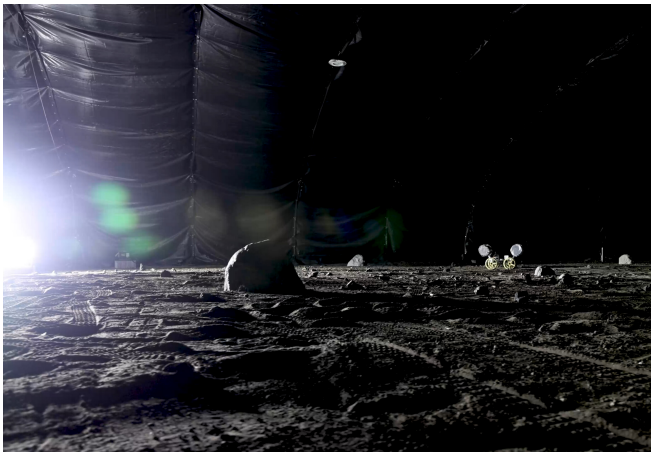

Figure 1: IPEx autonomously driving during TRL 5 mission demonstration in the test-site.

1. INTRODUCTION

NASA's goal of sustainable exploration of the Moon and Mars will be enabled by utilizing locally sourced resources such as oxygen. This approach will reduce the supplies launched from Earth and is known as in-situ resource utilization (ISRU) [1], [2]. Many of the resources available on the Moon can be found in the outer layer of loose rocky material called regolith. The regolith can be excavated and processed to extract the desired elements and may also be used directly as a construction material.

To date, NASA missions have only excavated tens of kilograms of lunar regolith [3]. Excavation has never been performed by a dedicated excavation technology/robot, rather only as a secondary function of an exploration rover or by an astronaut using scooping/sampling methods. The ISRU Pilot Excavator (IPEx) [4] will be NASA's first lunar surface robot specifically designed with the reliability and efficiency to excavate large quantities of regolith. This capability is critical to sustained lunar mission success. By the start of the next decade, the excavation needs will increase from sampling levels to tens or hundreds of tons of regolith per year [5], [6]. Going beyond this to full-scale sustained ISRU and construction of infrastructure will increase that amount to thousands of tons of regolith per year.

The IPEx project is developing a 30 kg-class excavator to demonstrate robotic excavation of large amounts (10,000 kg) of granular lunar regolith on a future technology demonstration mission (depicted in Fig. 2). IPEx uses novel excavation tools, called bucket drums, which are hollow cylinders with scoops staggered around the outside [7]. Regolith is collected with the scoops and flows into the drum where it is captured by an internal baffle system. The excavator can then transport the regolith in the drum and reverse the direction of the drum rotation to dispense the regolith. IPEx uses two sets of bucket drums that dig simultaneously in opposing directions which results in counter-acting excavation forces. This combination of bucket drum excavation tools and counter-acting excavation forces enables low mass robotic excavators to effectively dig in reduced gravity environments. This is a significant departure from terrestrial excavators that rely on high mass to produce tractive forces to counteract the forces of excavation.

IPEx is targeting excavation of 10,000 kg of granular lunar regolith as a demonstration of the capability that will be needed for a follow-on ISRU demonstration mission referred to as the "ISRU Pilot Plant". For the ISRU Pilot Plant to demonstrate extraction of 1,000 kg of oxygen, 10,000 kg of lunar regolith must be supplied to the ISRU system.

The notional mission would have IPEx prove the advancement in state-of-the-art for off-Earth excavation technology by excavating up to 10,000 kg of regolith, at a rate of 42 kg/hr, and covering a total distance of 70 km while operating in the south pole region of the Moon over 11 days during the local summer season. This mission profile keeps all operations during the lunar day which reduces thermal, lighting, and communications challenges. The work site will be in the area immediately surrounding the lander and covers approximately 750 m^2. IPEx will deploy from the lander, map the work area, then commence repeated excavation and traverse cycles in a supervised autonomous mode. During all phases, IPEx will use on-board cameras for localization and hazard detection. The lander, outfitted with fiducials, will be used as a navigational aid.

The lunar south pole (LSP) region presents several environmental challenges for this mission. The sun will be low on the horizon, casting long and dark shadows across the terrain while also washing out cameras pointed in its direction. Abrasive dust from the lunar regolith will cling to excavator surfaces interfering with mechanisms, radiators, cameras, and more. Another significant challenge is recreating these unique environmental conditions on Earth to effectively test and validate autonomous systems before deployment. Terrestrial testing of lunar technologies, particularly those designed for the south pole region, faces several hurdles. The low-angle lighting conditions are difficult to replicate over large areas while maintaining accurate shadow characteristics. The lunar regolith's physical and optical properties are challenging to simulate with terrestrial materials. In this work, we explore a terrestrial approach to testing IPEx and share preliminary results and datasets. We introduce the IPEx autonomy test-site, shown in Fig. 1, a large-scale enclosed environment designed to approximate key visual and operational aspects of the LSP. This facility enables the development and validation of autonomous excavation technologies in a controlled, yet representatively challenging setting. The key contributions of this work include:

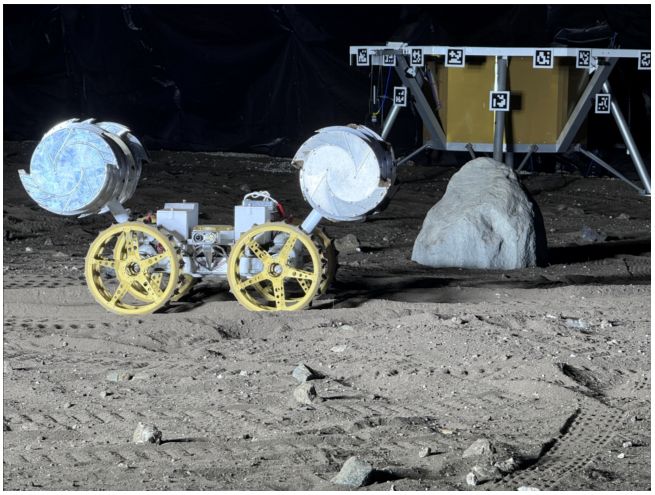

Figure 2: IPEx in its 'alpha' configuration with surrogate hardware, driving near a large rock in front of the mock lander.

1. A detailed description of the LSP terrestrial test environment, including lighting simulation, terrain preparation, and mock lander integration.
2. Preliminary results from a mock mission conducted in the test environment using the IPEx platform.
3. Annotated datasets created at the test-site. These datasets include annotated imagery for the development and benchmarking for vision-based object detection systems, photogrammetry, and localization. The datasets will be available at [8].
4. Insights into the challenges and limitations of terrestrial testing for LSP missions, and proposed strategies to address these limitations.

The remainder of the paper is organized as follows. Section 2 provides an overview of the LSP environment and a discussion of its unique geographical and lighting characteristics. Section 3 details the IPEx autonomy test-site including its physical layout, lighting system, terrain features, and communication infrastructure. Section 4 presents the results of a Technology Readiness Level 5 (TRL 5) [9] mission demonstration conducted in the test-site. Section 5 introduces the autonomy datasets collected in the test environment and discusses their potential applications. Finally, Section 6 concludes the paper with a summary of findings and avenues for future work.

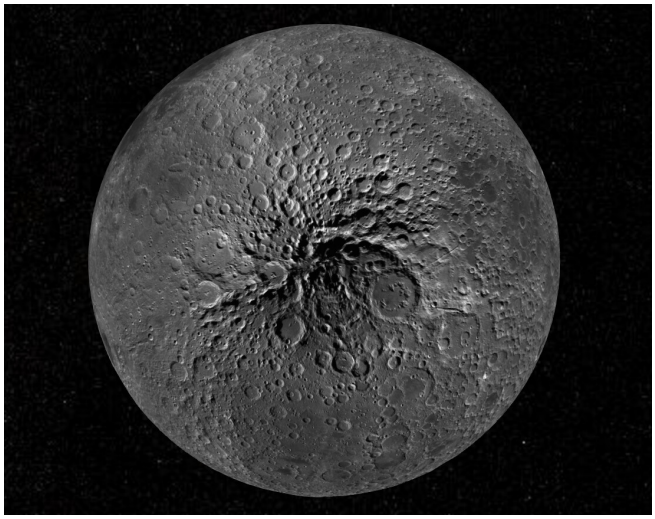

Figure 3: A 3D projected view of the lunar south pole from JPL's MoonTrek.

2. THE LUNAR SOUTH POLE

The Lunar Surface

The LSP is predominantly a highlands environment, characterized by a thick layer of regolith covering the surface. This regolith, a product of billions of years of meteorite impacts, is composed of fragmented rocks, soil, and dust. At the LSP, as in other highland areas, the median regolith depth is estimated to be 10–15 m, which is significantly deeper than the 3–5 m typically found in mare regions [10]. This extensive regolith layer plays an important role in shaping the surface properties and interactions at the LSP. A reconstructed orbital view of the LSP is depicted in Fig. 3.

The regolith particles at the LSP exhibit specific characteristics that influence the surface's behavior. Lunar soil particles are generally angular and irregular in shape, a result of the impact processes that form them. The size distribution of these particles is broad, ranging from fine dust less than 10 μm in diameter to coarse grains and rock fragments.

Of particular importance are the particles smaller than 20 μm, which are highly susceptible to electrostatic forces due to their high charge-to-mass ratios [11]. This property contributes to the potential for dust lofting and adherence to surfaces including lenses, which can be a significant consideration for selecting appropriate sensors. In this work, we primarily focus on representing the visual effects from camera-based systems.

Solar Lighting

The LSP presents distinct and challenging lighting conditions primarily driven by the Moon's axial tilt of approximately 1.54° relative to the ecliptic plane [12]. This small tilt causes the Sun to remain low on the horizon throughout the lunar day, with a maximum solar elevation angle of only about 1.5° directly at the pole [13], [14]. These unique lighting characteristics necessitate careful consideration in the design of vision-based autonomy solutions for surface operations. Depending on the landing position, lunar days, under these conditions, may last several Earth weeks.

At latitudes near the lunar pole, solar angles fluctuate based on both latitude and time within the lunar cycle. For instance, at 89°S latitude, the maximum solar elevation reaches around 2.5° during the summer solstice, while at 85°S latitude, the Sun can rise as high as 6.5° [15], [16]. These low-elevation angles can significantly influence mission planning for both crewed and uncrewed robotic missions as the surface becomes more dimly lit while risks of eye (or sensor) damage increase as the Sun remains at the horizon, instead of appearing overhead and out of direct sight.

One of the most significant consequences of the low solar angles is the extreme length of shadows. As the Sun barely rises above the horizon, objects cast shadows that are many times their own height. The shadow length L can be calculated as

$$L = \frac{H}{\tan(\theta)},$$

where H is the height of the object and θ is the solar elevation angle. For example, a 1 m tall object at 89°S during the summer solstice casts a shadow approximately 23 m long. This has profound implications for vision-based navigation, as shadows can obscure important terrain features or be misinterpreted as obstacles by the vision systems.

In addition to the long shadows, the surface of the Moon experiences extreme contrast between illuminated and shadowed regions that makes it difficult for conventional imaging systems to capture details in both the bright and dark areas simultaneously. This high contrast often results in loss of information in shadowed areas, where hazardous terrain features may be occluded.

Figure 4: Apollo 12 Astronaut Alan Bean carrying the Apollo Lunar Surface Experiment Package (ALSEP) with the Sun in view.

A key aspect of the LSP lighting environment is the intensity and position of the Sun. Due to the lack of atmosphere on the Moon, sunlight is unattenuated, resulting in bright illumination. With the Sun appearing low on the horizon, it would often be in direct line-of-sight for astronauts or

imaging systems at the LSP. This can lead to significant glare and potential temporary blindness when looking towards the Sun, as illustrated in Fig. 4. The bright, unfiltered sunlight also poses risks for imaging systems.

The presence of permanently shadowed regions (PSRs) adds another layer of complexity to the lighting environment at the LSP. These regions, typically located in the floors of craters, never receive direct sunlight due to the low solar angles and the surrounding topography. Temperatures within these PSRs can be as low as 40 K during lunar summer, making them some of the coldest known places in the solar system [17].

Illumination Levels— At the lunar surface, the total solar irradiance is approximately 1361 W/m^2 [18]. However, the low solar elevation angles significantly reduce the amount of irradiance on a horizontal surface such as the surface terrain, as it depends on the angle of incidence. This reduction can be modeled using the cosine law of illumination

$$E_h = E_0 \cos(\theta),$$

where E_h represents the horizontal irradiance, E_0 is the total solar irradiance, and θ is the solar zenith angle (equal to $90^\circ - E_s$, where E_s is the solar elevation angle). For instance, at 85°S latitude during the summer solstice, where the solar elevation angle reaches approximately 6.5°, the horizontal irradiance is calculated as

$$E_h = 1361 \cdot \cos(83.5^\circ) \approx 154\,\text{W/m}^2.$$

Under these same conditions, vertical faces such as the sides of a lander will be subject to a much higher irradiance. Vertical irradiance can be calculated as

$$E_v = 1361 \cdot \cos(6.5^\circ) \approx 1352\,\text{W/m}^2.$$

This difference in horizontal and vertical irradiance create a high-contrast environment that can be challenging to image. It is important to recreate the high-contrast conditions between horizontal terrain and vertical faces of the lander to ensure that the chosen camera parameters and exposure adjustment subsystems allow for properly exposed images of the terrain, surface features, and assets.

Because the IPEx rover uses the lander as a landmark to compute an absolute pose estimate, the quality of the lander imagery is of high priority. In such lighting conditions, autonomous systems must be equipped with advanced imaging technologies, including high dynamic range sensors, to compensate for the low light levels and wide contrast ranges. They may also employ various automatic exposure adjustment algorithms to adapt to changes in lighting conditions.

Apollo Imagery—While none of the Apollo missions targeted the lunar poles, Apollo 12's extravehicular activities (EVAs) provide insights into the lighting conditions expected at the LSP. Apollo 12's first EVA occurred under a solar elevation angle of 7.5° to 9.5° [19], which is near the low solar angles anticipated during future LSP missions. One of the most striking features observed in Apollo 12 imagery is the length of shadows, particularly those cast by astronauts and lunar surface equipment. Shadows extended several meters which complicates the interpretation of the terrain and has the secondary effect of masking surface features. Fig. 5 offers an example of the impact of long shadows.

Figure 5: A second view of Apollo 12 Astronaut Alan Bean carrying ALSEP. The low solar light casts a long shadow off the suit (right).

The Apollo missions identified a significant depth perception challenge faced by astronauts on the lunar surface. The absence of recognizable features, such as trees or buildings, limited the context clues necessary for accurately judging distances to unfamiliar terrain. This issue also affects stereo vision systems used by robots, as the largely featureless landscape provides few reference points. Coupled with the intense solar glare, which stays low on the horizon, operating on the Moon becomes even more difficult. Replicating these unique conditions on Earth presents additional difficulties due to atmospheric effects.

Surface Features

Large rocks are relatively scarce on the lunar surface, typically covering less than 1% of the surface area [10]. However, some areas show higher rock abundance, where certain regions may have 10% to 20% of their surface covered by rocks. These rocky regions are not uniformly distributed and tend to concentrate around "fresh" craters and elevated areas, making the rock distribution highly localized. In terms of surface features, the surface is dominated by craters, both large and small, with a variety of depths and morphological characteristics. These craters significantly impact the geological and geomorphological landscape and result in rugged terrain that is challenging to navigate.

Surface slopes of the lunar surface are also influenced by the crater density and distribution, with global slope distributions varying depending on the region. Crater size-frequency distributions, particularly for smaller craters, follow generalized patterns, though local variations can be considerable. The topography of the LSP is presumed to be more rugged than other lunar regions due to the highlands environment, with some craters featuring steep walls and complex inner structures. The inclusion of craters at the IPEx autonomy test-site is an ongoing effort.

Figure 6: Front exterior of the test-site tent. A Ubiquiti AirFiber radio used to communicate with the ground is shown in the center.

3. The Autonomy Test-Site

Site Selection

The initial requirements driven by the IPEx rover concept of operations (ConOps) dictated that the site be large enough to allow the rover to perform simulated lunar travel paths with minimal overlap of previous paths. Additionally, the site needed to provide sufficient space to accommodate a mock lunar lander, obstacles, and simulated solar lighting system within the test area. A staging area near the test-site was also required for test support equipment. A trade study was performed, considering sites on Kennedy Space Center (KSC), Cape Canaveral Space Force Station (CCSFS), and in the local areas off center. Logistically, KSC proved to be the best option.

A follow-on trade study comparing available real estate at KSC, while simultaneously considering existing buildings, led the team to settle on an open area approximately 183 m east of the office building where the early IPEx team offices were being established. The next decision to be made was determining the size of the test area on that plot of land. The search began for an affordable, rapidly constructed structure that would meet KSC center building requirements and satisfy IPEx testing needs.

Facility

The facility design for the IPEx test-site was driven by several key requirements and environmental considerations. Primarily, the interior needed to remain dark to simulate lunar "sky" conditions, allowing for the most effective use of artificial solar lighting. The Florida climate also played a significant role in the facility selection, with humidity, rainfall, moisture accumulation, and lightning protection being crucial factors.

Various facility options were considered, including lean-to structures, brick and mortar buildings, multiple portable structure options, and hybrids such as CONEX box walls with fabric or rolled steel arch roofs. The chosen facility had to meet KSC building requirements, including hurricane rating and compliance with Authority Having Jurisdiction fire and exit regulations, as well as approval from a wide array of stakeholders.

After careful consideration, the IPEx team selected a fabric-covered, galvanized tube design provided by a large, reputable manufacturer widely used for similar structures at KSC, CCSFS, and globally. This is shown in Fig. 6. The procured tent measured 39.6×21.3 m with a 1.8 m sidewall height to allow easy walk-through on the edges, and a 6.1 m ridge height. This ridge height was sufficient for testing requirements without unnecessary elevation, which would have increased costs.

To darken the interior, the team designed a scheme where black tarps could be easily suspended from the tubular trusses that run the width of the tent every 3 m. Split curtains at either end of the tent divide the practice area from the staging areas (referred to as "foyers") for testing equipment. The foyer curtains or end panels were designed to be sealed in the center with black Velcro, allowing for easy access and resealing.

The panel material for both the interior and end panels is a 95% light-blocking polyester weave. While more opaque options were available, they came with a 40%+ price increase over the selected material. With the end panels in place and foyers sectioned off, the rover practice area measures 33.5×21.3 m. The blackout panel drapes down from the ridge height approximately 25 cm in the center of each panel.

Terrain

The terrain within the test facility is composed of local Florida soil. Although no lunar simulant was used, the soil was prepared to simulate key aspects of the lunar surface environment. During the preparation process, rocks larger than 7.6 cm in diameter and all vegetation were removed, resulting in a mostly uniform surface texture, akin to plowed earth. This "fluffy" texture was chosen to approximate the loose, fragmented nature of lunar regolith at the LSP. Using a lux meter to measure illuminance, the test-site's albedo was measured to be an average of 0.26. This is higher than the measured albedo of the lunar surface of 0.11.

Figure 7: A close-up view of the terrain in the test-site. Several rocks are in view in addition to the imprints from IPEx's wheels.

Due to operation in Earth's gravity, replicating the granular properties of the LSP remains a challenge. Using regolith simulants, such as LHS-1, was considered but not pursued due to the logistical, financial, and safety challenges it would introduce to the facility. Using Florida soil eliminated those

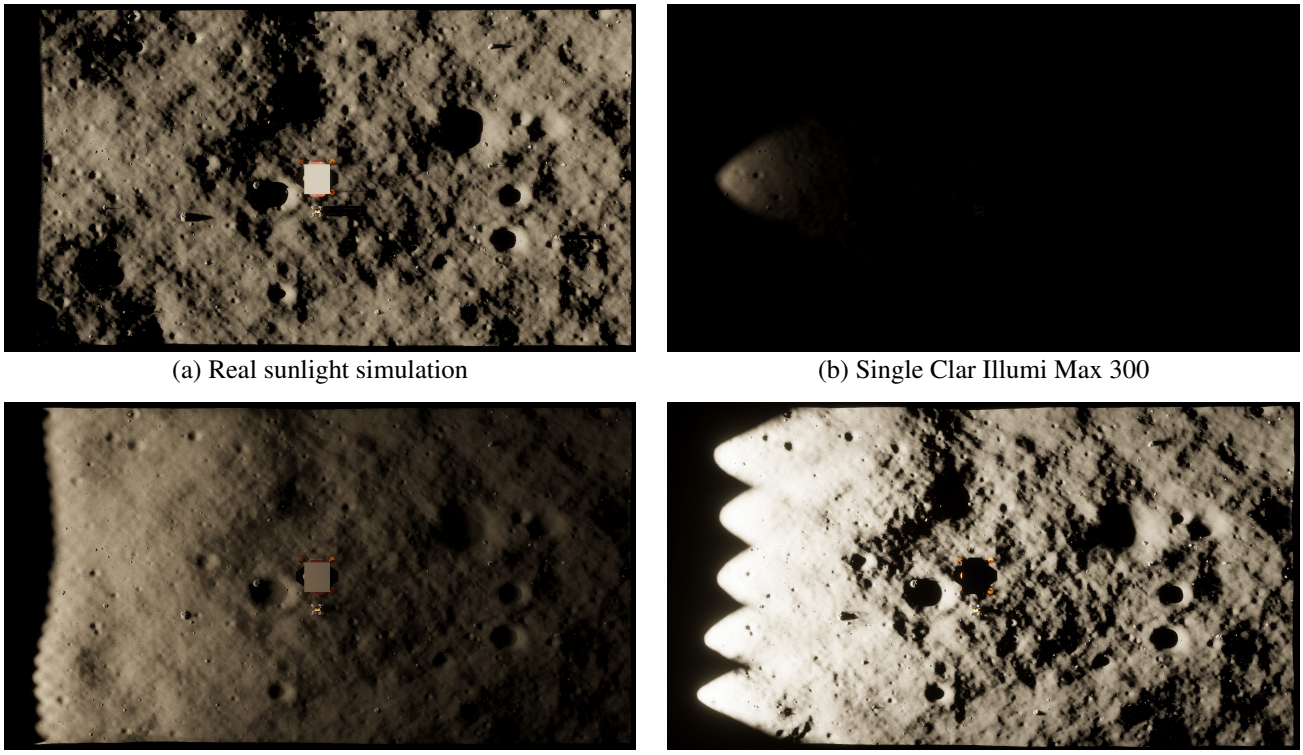

(a) Real sunlight simulation

(b) Single Clar Illumi Max 300

(c) Multiple lights (48) configuration

(d) HMI lighting solution

Figure 8: Comparison of different lighting configurations simulated for the test-site with a locked exposure: (a) Real sunlight simulation, (b) Single Clar Illumi Max 300 light, (c) Multiple lights (48) configuration, and (d) HMI lighting solution.

concerns while still providing a test bed that allowed for assessment of IPEx's ability to traverse and excavate a challenging terrain.

To further characterize the terrain, a series of penetration tests were conducted using a Geotester Pocket Penetrometer after the completion of the TRL 5 demonstration, discussed in Section 4. These tests aimed to assess the soil compaction levels at different stages of rover operations. The results revealed that driving over the terrain significantly compacts the soil, with areas subject to repeated traffic showing compaction values up to twice those of undisturbed soil.

More notably, excavation activities in the dig site increased soil compaction by as much as 11 times from a baseline 0.5 kg/cm^2, while soil in the dump site experienced a reduction in compaction by a factor of 2.5. These findings indicate that over the course of a mission at the LSP, the dig sites are expected to become increasingly compact, posing a growing challenge for excavation operations, while dump sites may become progressively looser, affecting material handling and stability.

Lighting

Accurately recreating the lunar lighting conditions expected at the poles presented significant challenges. The LSP environment is characterized by extreme contrasts: areas of perpetual shadow coexist with regions of near-constant illumination, while the Sun never rises more than a few degrees above the horizon [16]. This unique lighting scenario creates long, sharp shadows and high-contrast scenes that are difficult to replicate terrestrially.

Our primary challenge was to achieve uniform illumination over a large area while maintaining the crisp, elongated shadows characteristic of the lunar poles. This required balancing two often conflicting goals as the installation of additional lights would improve uniformity while sacrificing the sharpness of shadows. To address this, we developed a 3D lighting simulation using the Unity Engine [20] with the high definition rendering pipeline (HDRP), which allowed us to model and evaluate multiple lighting configurations before physical implementation.

The HDRP package enabled us to specify lighting configurations based on physical lighting units and measure the output in the simulation to assess the uniformity and shadow sharpness. The resultant illuminance is plotted and was used to visualize multiple lighting fixtures and layouts before procuring or reconfiguring the large physical lights in the test-site. By adjusting lights and prioritizing different visual conditions, a series of tests can be conducted to allow testing vision systems across a range of conditions.

To compare the lighting configurations, we simulated several scenarios. Fig. 8(a) shows a simulation of real sunlight at the lunar surface, which provides a baseline for comparison. We then tested various artificial lighting setups based on lights authorized for use. A single Clar Illumi Max 300 LED light configuration (Fig. 8(b)) proved effective for short-range testing but lacked coverage for larger areas. The Clar light is a 5600K light capable of 132,000 lux at 0.5 m.

To improve coverage and uniformity, we simulated a configuration with 48 lights (Fig. 8(c)). While this improved overall illumination, it sacrificed shadow quality. We also evaluated a metal halide solution based on the ARRI Daylight

18 kW lights (Fig. 8(d)), which provided extremely bright illumination with fewer lights but was costly and challenging to integrate. Ultimately, we settled on a middle approach, using six RuggedGrade 1400W StadiumPro IV lights with 5000K color temperature, producing 200,200 lm at 143 lm/W. These lights, depicted in Fig. 9, were chosen with a 20° beam angle, the narrowest offered, to improve the sharpness of shadows.

Figure 9: The six RuggedGrade StadiumPro IV 1400W lights used as solar simulators in the test-site.

Based on this lighting configuration, we measured the following lux measurements across the test-site. At 30 cm from the lights, we measured 78,000 lux on the ground plane, and 192,000 lux vertical to the light. The front face of the largest rock nearest the lights (depicted in Fig. 12 in the center of the right image) measured 9,500 lux. At the foot of the lander, we horizontally measured 360 lux and 2,345 lux vertically. Finally, at the far side of the tent, parallel to the ground measured 94 lux and vertically 850 lux. These measurements reveal the steep falloff in light intensity with distance. Instead, it creates significant variability in brightness levels across the test area. While this non-uniformity poses challenges for consistent imaging, it provides an opportunity to test adaptive exposure algorithms as the rover navigates between the brighter near side and the dimmer far side of the tent.

Mock Lander

The mock lander used in the test-site is 2.75 m in diameter and 1.2 m tall. It serves as a visually acceptable stand-in for future lunar missions. The lander is colored to simulate the appearance of a flight lander, with a white top deck, gold metallic sides, and silver metallic landing legs. This is depicted in Fig. 10.

Mounted on the lander are AprilTag fiducials [21], which IPEx uses to acquire absolute pose with respect to the lander. The fiducials are mounted along the top perimeter edges and approximately at the middle of the lander legs and angle support beams. The fiducials are 15.24×15.24 cm in size and belong to the 36h11 family, with the black-to-black edge measuring 12.1×12.1 cm. There are a total of 16 AprilTags on the lander. The AprilTags were painted onto polycarbonate sheets using flat white vinyl for the background and Musou black acrylic paint for the black areas. This ultra-black paint provides up to 99.4% light absorption, ensuring high contrast between the white border and the black interior of the AprilTag while also eliminating glare from the solar simulator in the test-site.

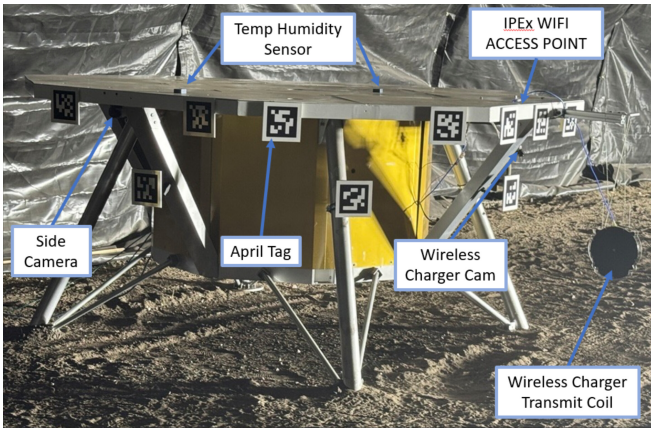

Figure 10: The full-scale mock lander used for the autonomous docking and localization.

The lander is equipped with a networking switch that connects to the flight control room network. IPEx's Wi-Fi communications are routed through an access point on the lander. For verification of localization and docking, the lander provides three camera views. All three cameras are fixed to the lander with fixed focus and focal length. Two side-facing cameras are oriented towards the dig and dump sites, while a front-facing camera is angled downwards for wireless charging docking verification.

The lander cameras are FLIR BlackFly S BFS-GE-88S6-M camera boards with Kowa LM6JC 2/3" 6 mm C-mount lenses. During the TRL 5 IPEx demonstration, the lander side cameras were not initially used, assuming that the IPEx team might not have unlimited access to these cameras for the full duration of the mission. The wireless charger docking camera was used solely to visually confirm that IPEx had completed its docking routine. The wireless charger transmit coil is mounted offset from the front face of the lander and is suspended by cables. This configuration ensures that IPEx cannot damage itself or the transmit coil during an off-nominal docking attempt.

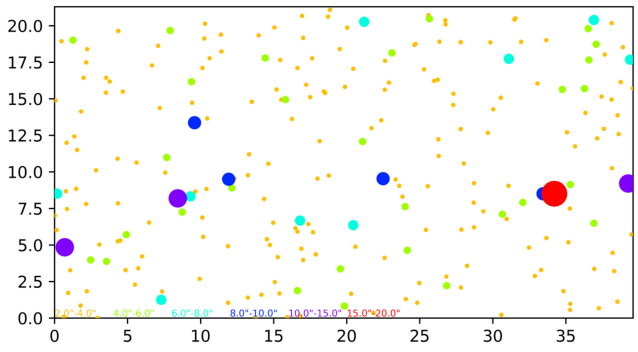

Figure 11: Plot of rock distributions used in the test-site. The size of the circle corresponds to the size of rock used for physical testing.

Figure 12: Side views from the cameras positioned at the test-site.

Surface Features

Understanding the distribution of rock sizes on the lunar surface is crucial for assessing potential hazards to landing spacecraft and surface operations. [22] provides insights into block distributions at various Surveyor landing sites, which can inform our expectations for LSP landing sites. The distribution of rock sizes on the lunar surface typically follows a power law model. While the original study focused on Surveyor I, III, VI, and VII sites, we can use the Surveyor VI data as a representative model for our purposes at the LSP.

In the model, a is the coefficient that relates to the overall abundance of rocks, while b is the exponent that describes how quickly the number of rocks decreases as their size increases. Specifically, $a = 0.154$ represents the relative abundance of rocks, and $b = -2.286$ indicates the steepness of the size-frequency distribution, with more negative values corresponding to a steeper decline in the number of larger rocks. The number of rocks per square meter between the sizes d_{min} and d_{max} can be estimated:

$$N = a(d_{min}^{b} - d_{max}^{b})/100 \quad (1)$$

where N is the number of rocks per square meter, and d is the rock diameter in meters. It is important to note that this model was derived from measurements of smaller rocks (typically < 1 m) visible in Surveyor photography. [22] revealed that extrapolating this distribution to larger rock sizes (> 2.5 m) visible in orbital photography often overestimates the actual density of large blocks. This suggests that the overall shape of the cumulative lunar block population may be nonlinear, with different slopes over different size intervals.

To recreate these rock distributions in our test environment, we binned rocks into discrete size ranges based on the power law distribution. Rocks were then positioned randomly within the test-site, approximating the calculated spatial density for each size range. This approach allows us to simulate a realistic lunar surface environment while acknowledging the limitations of our current understanding of large block distributions. This is depicted in Fig. 11.

It is worth noting that rock distributions can vary significantly. For instance, [22] found that the Surveyor VII site, located in the lunar highlands near Tycho crater, had a much higher density of large blocks compared to the mare sites. While we based the distribution on Surveyor VI data, future missions to the LSP may encounter different distributions due to the unique geological history of the polar regions.

Communication

The test-site is wirelessly linked to the control building via Ubiquiti AirFiber radios. To avoid saturating this link with camera data, a server was installed local to the test-site, and is used to ingest all situational awareness imagery locally. This server also runs the OptiTrack motion tracking software and the network video recorder software for logging the situational cameras. This way only tracker position data and compressed situational imagery needs to be sent over the AirFiber link leaving as much bandwidth as possible for rover operations.

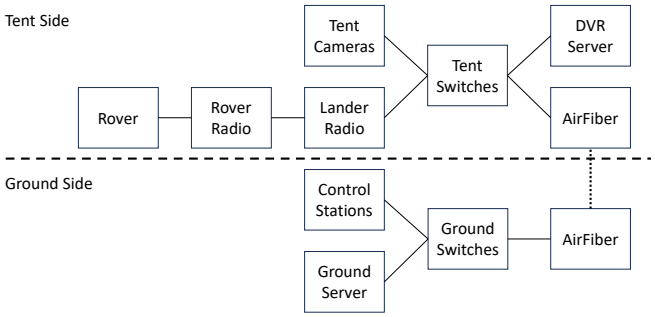

Figure 13: The network topology used for ground and test-site communication.

The lander is equipped with a network switch to allow communications through the lander radio, multiple lander cameras, and temperature/humidity sensors installed throughout the test-site. All networking infrastructure is protected from power outages via a set of uninterruptible power supplies. A high-level overview of the network topology is depicted in Fig. 13. The test-site is configured with two types of situational cameras to aid developers and provide real time info for the out-of-sim operators:

- Four Axis security cameras are used to provide real time color imagery of the test area to operators. Three of these cameras are Q6128-Es and have pan-tilt-zoom (PTZ) capabilities. Two PTZs are mounted to the ceiling of the in the front corners. One PTZ is mounted to a tripod on the ground that can be placed anywhere in the tent to provide other perspectives as required. The fourth camera is an M3058-PLVE fixed camera at the center of the tent's ceiling with a fisheye lens. This view provides an overview of the entire field layout.
- 36 OptiTrack Slim x13 cameras are placed around the perimeter of the test area. A tracking beacon on the rover

Figure 14: Overhead situational camera view with manual de-warping applied to the image. Note the sharpeness and length of shadows.

is tracked by these cameras and the pose data is published on a Robot Operating System (ROS) topic to provide a ground truth pose to the out-of-sim operators in real-time. Because the data is sent via a ROS topic, it can be recorded with the rest of the rover's telemetry in a time series database. During testing, operators can use the OptiTrack data as ground truth for testing localization strategies.

4. TRL 5 Mission Demonstration

The IPEx autonomy test-site has been instrumental in supporting autonomy software development and has enabled the IPEx team to demonstrate the excavator's capabilities within its mission ConOps over a multi-day period.

Preliminaries

Beginning on August 25th, 2024, IPEx underwent a five-day continuous TRL 5 ground demonstration. The objective was to perform 334 excavation and unload cycles at the test-site, simulating the proposed lunar mission and serving as a baseline for ConOps timing. This demonstration was designed to validate the complete system, including mechanical and actuator subsystems, surrogate avionics, and software required to complete the nominal mission.

In the mock mission, the robot was instantiated on the surface in a post-deployment configuration to immediately commence a mapping phase. During the mapping phase, the robot collected several images from four cameras that were downlinked to the ground and used to generate a map of the local terrain. Following this, the map was imported into the ground operator consoles, such as those shown in Fig. 15, and marked the start of the operational mission. The operators then identified safe paths between the excavation and unload areas, and back to the wireless charger located on the mock lander. Based on this, a path was uplinked to the robot for it to commence cycling between the excavation and unload sites.

Test-Site Operations

The test-site was configured to simulate LSP conditions. A statistically accurate distribution of rocks was placed in the test area, unknown to the operators, to simulate the challenging terrain. Low solar angle lighting was provided by stadium lights to replicate the harsh illumination conditions found at the LSP. To simulate communication with a Commercial Lunar Payload Services (CLPS) lander to ground, the team implemented reduced data transmission and a 14-second round-trip delay. All equipment in the test-site operated continuously throughout the demonstration period without any power outages.

The robot used in the demonstration is the 'alpha' configuration of the TRL 5 hardware with some modifications to make it more suitable for terrestrial testing, including larger and externally mounted battery packs and surrogate avionics setup based on the final avionics computer. All localization and autonomy software ran on-board the robot, with a subset of the imagery and telemetry downlinked for ground operators.

Figure 15: Operators observing robot during its traverse to the excavation site.

Ground Operations

The robot was remotely operated by four shifts of ground crews over the course of the mock mission. Each crew consisted of four personnel: a primary operator, a secondary operator, a telemetry desk officer, and a simulation coordinator (sim-c). The primary operator controlled the robot during nominal operations and led deliberations in the event of an issue, while the secondary operator provided support, tracked performance, and aided in troubleshooting. The telemetry desk monitored and analyzed incoming data, and the sim-c oversaw the simulation with real-time data and imagery, and carried out all sim-c operations such as replacing batteries to limit the amount of real downtime. Only the sim-c operators had access to the situational cameras.

Ground control was situated in the IPEx flight control room, located 183 m from the test-site. The setup included four telemetry displays running off the flight control computer for in-sim operations, and a separate computer for the sim-c operators with access to the real-time, non-lunar link delayed telemetry and imagery.

Results

Operational Performance—The robot operated continuously for 77 hours and 46 minutes, which, after accounting for thermal resets and wireless charging events, translated to 205 hours and 18 minutes (approximately eight days) of mission time. Over the course of the demonstration, the robot traversed a total of 58.1 km across 334 mission repetitions

Class	Instances	Avg. Pixels/Mask		Pixel Area Percentile			
		Mean	Std. Dev	25th	50th	75th	90th
Lander	442	330,009.51	50,123.12	120,280.30	200,372.60	469,379.31	726,144.27
Rock	7,171	35,357.90	4,789.21	2,155.27	6,308.50	23,697.51	83,023.22
Fiducial	1,425	2,880.20	750.45	999.99	1,659.98	3,610.51	5,752.85
Fiducial Inverse	1,467	2,361.01	678.91	828.03	1,431.99	3,236.53	5,599.64

Table 1: Dataset statistics including class, instances, average pixels per mask with mean and standard deviation, and pixel area percentiles.

between excavation and dump sites. It achieved a maximum sustained drive speed of 40 cm/s. The robot also completed 35 automated docking and recharge procedures, with an average of 10 repetitions per battery charge.

Each mission repetition followed a defined autonomous cycle: three drives between the excavation and dump zones (covering approximately 100 m each way), followed by the excavation and unloading of regolith, and finally three more drive cycles. On average, each repetition took nine minutes to complete. Every 10 repetitions, the robot performed a thermal reset and an automated docking sequence with the lander to recharge its batteries. The robot performed efficiently throughout, completing the demonstration with 59 hours of operational margin.

Throughout the demonstration, the robot generated and transmitted telemetry to the ground control station. This data included localization estimates, actuator status, low-resolution engineering imagery, and command statuses. Ground control systems meticulously logged all communications with the robot, enabling the IPEx team to assess system performance under representative delays and limited bandwidth.

Figure 16: IPEx unloading at the 'dump' site. Note trail of granular material exiting bucket drum scoops.

This successful demonstration not only validated the current system but also provided valuable insights for refining the functionality and robustness of the software and hardware systems for the next stage of development at TRL 6. From this work, we also generated the datasets that we describe below.

5. Test-Site Autonomy Datasets

Throughout the tests conducted in the test-site, several datasets have been collected to support autonomy algorithms development. This includes instance segmentation datasets for recognizing objects within the images, imagery datasets for mapping the terrain, and ROS bags, which can be played back with time stamps to facilitate lander recognition algorithm development and other localization tools such as for visual odometry.

Instance Segmentation Dataset

The instance segmentation dataset was collected using a pre-IPEx surrogate robot based on the Clearpath Robotics Husky unmanned ground vehicle. Included on the robot were prototype IPEx camera sensors based on the FLIR Blackfly S cameras and 6 mm Kowa lenses. This is similar to the camera configuration used on the mock lander. To collect the dataset, the surrogate robot was driven in arching and 'figure-8' patterns near the mock lander.

The mock lander includes several fiducial markers based on the WhyCon fiducial system [23]. For our testing, a custom fiducial detector was devised with the ability to delineate between a standard fiducial and an inverted fiducial. This dataset will be made available at [8].

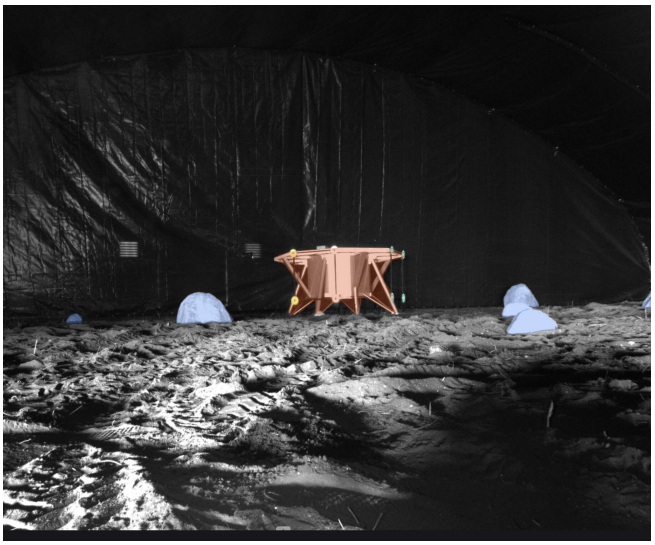

Figure 17: Example of annotated image from the instance segmentation dataset.

Annotation Process— All images in the dataset have been manually annotated, with annotations including both bounding boxes and pixel-wise segmentation masks. This allows for a range of computer vision tasks such as object detection, semantic segmentation, and instance segmentation. The annotations were created using the computer vision annotation

tool (CVAT) [24]. Trained annotators were tasked with labeling each instance in the dataset. Segment Anything Model [25] was used as a serverless function within CVAT to facilitate labeling. In the case of images with heavy shadows, some manual correction was necessary.

Figure 18: Example image from mapping dataset of IPEx's camera facing towards the simulated sun.

Dataset Composition—The dataset comprises a total of 2,343 images, with annotations covering four distinct classes relevant to IPEx's testing scenarios: lander, rock, fiducial, and fiducial inverse. In total, 10,505 instances have been annotated across all images. Table 1 provides a detailed breakdown of the dataset's statistics, including the number of images and instances for each class, the average pixel area per mask, and pixel area percentiles.

Photogrammetry Dataset

Another dataset was recorded for the purposes of a mapping phase, during the TRL 5 demonstration. This dataset includes 1514 images captured from four distinct cameras on synced intervals every 0.5 m of linear driving during the mapping phase of the mock mission. One such example image is shown in Fig. 18.

As the robot carries cameras on all sides, four orthogonal views were downlinked. The cameras are based on the IDS GV-51F1SE consisting of a Sony IMX547 sensor with a binned resolution of 1230×1028 pixels for the front and rear sets of stereo pairs, and a resolution of 2460×2056 pixels for the two side cameras. All images collected are monochromatic although the cameras are capable of producing color.

The side cameras used a custom auto-exposure routine implemented to expose to the lander fiducials during arch-like driving patterns. The stereo cameras were set to the hyperfocal distance, while the side cameras were manually focused to track the lander from a 7 m driving radius. The images have been used to generate ground-based maps using structure from motion algorithms such as COLMAP [26] and neural radiance fields [27] which have also been demonstrated on simulated lunar terrains [28]. An example point cloud from COLMAP is shown in Fig. 19.

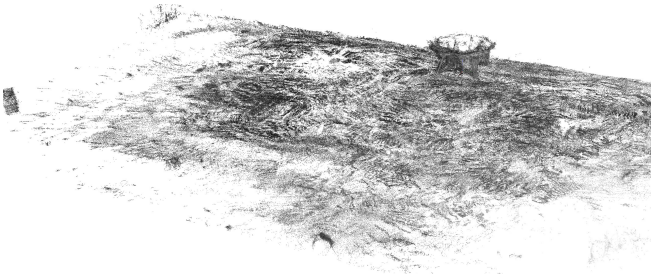

Figure 19: Example point cloud from the test-site generated using COLMAP.

6. CONCLUSION

The IPEx autonomy test-site represents a significant effort towards terrestrial testing of lunar excavation technologies. Through careful design and implementation, we have created an analog that approximates the unique lighting conditions, surface features, and operational challenges expected at the LSP.

Our test-site incorporates several key elements, including a high-power lighting system to approximate the high-contrast illumination characteristic of the LSP, a terrain composition that mimics the visual properties of the surface, and a full-scale mock lander that serves multiple purposes. We also included a distribution of rocks and other surface features based on lunar data, along with monitoring and data collection systems for quantitative evaluation during and after the tests.

The successful completion of a five-day TRL 5 mock-mission supports the test-site's capability for extended simulations. This demonstration not only tested the functionality of the IPEx system but also provided several insights for the robot's hardware, software, and human factors. The datasets generated during our testing, including instance segmentation data and photogrammetry information, may prove useful for the development of autonomous navigation and excavation algorithms for future missions.

While the test-site provides a new platform for terrestrial lunar testing, it also highlights areas for improvement. Future work could focus on improving the fidelity of the simulated environment. This might include the incorporation of more diverse terrain features, such as craters of various sizes and regolith simulants, which were not included in this iteration.

We also plan to conduct discrete light tests to further refine our understanding of the impact of different lighting conditions on autonomous operations (such as varying the solar elevations and azimuths). Additionally, testing with other sensor configurations could provide valuable comparative data and help validate the test-site's versatility. These additions aim to further reduce the risks associated with deploying new ISRU technologies at the LSP.

ACKNOWLEDGMENTS

We thank the many team members and government personnel who assisted with the construction and operation of the facility, particularly Frank Kline, John Lahl, Nathan Gelino, Musashi Howe, and others. Thanks to Ben Hockman for his insights on rock distributions and Gary Holmgren for his effort with the datasets.

REFERENCES

[1] G. B. Sanders, W. E. Larson, K. R. Sacksteder, and C. A. Mclemore, "NASA in-situ resource utilization (ISRU) project: Development and implementation," in *Proceedings of the AIAA SPACE Conference & Exposition*, 2008, p. 7853.

[2] G. B. Sanders, "Advancing in situ resource utilization capabilities to achieve a new paradigm in space exploration," in *Proceedings of the AIAA SPACE and Astronautics Forum and Exposition*, 2018, p. 5124.

[3] G. Heiken, D. Vaniman, and B. M. French, *Lunar Sourcebook: A user's guide to the Moon*. Cambridge University Press, 1991, no. 1259.

[4] J. M. Schuler, J. D. Smith, A. J. Nick, B. C. Buckles, J. E. Dyas, V. V. Ortega, J. M. Cloud, A. G. Dokos, E. L. Zhang, J. J. Wang, M. A. Baron, T. J. Muller, C. J. Clark, and M. W. Howe, "ISRU Pilot Excavator (IPEx) technology readiness level 5 design overview," in *Proceedings of the AIAA Accelerating Space, Commerce, Exploration, and New Discovery Conference*, 2024, p. 4890.

[5] G. B. Sanders, W. E. Lason, K. R. Sacksteder, C. Mclemore, and K. Johnson, "NASA in-situ resource utilization (ISRU) technology and development project overview," in *Space Technology Applications International Forum*, 2008.

[6] M. F. Palos, P. Serra, S. Fereres, K. Stephenson, and R. González-Cinca, "Lunar ISRU energy storage and electricity generation," *Acta Astronautica*, vol. 170, pp. 412–420, 2020.

[7] R. P. Mueller, J. D. Smith, J. M. Schuler, A. J. Nick, N. J. Gelino, K. W. Leucht, I. I. Townsend, and A. G. Dokos, "Design of an excavation robot: regolith advanced surface systems operations robot (RASSOR) 2.0," in *Proceedings of the ASCE Conference on Engineering, Science, Construction, and Operations in Challenging Environments*, 2016, pp. 163–174.

[8] ISRU Pilot Excavator, "Lunar south pole test-site datasets," 2025, dataset release will be linked here. [Online]. Available: https://nasa.gov/isru-pilot-excavator/

[9] W. M. Kimmel, P. M. Beauchamp, M. A. Frerking, T. R. Kline, K. K. Vassigh, D. E. Willard, M. A. Johnson, and T. G. Trenkle, "Technology readiness assessment: Best practices guide," 2020.

[10] F. B. Leahy, "SLS-SPEC-159, cross-program design specification for natural environments (DNSE) Rev. I," Tech. Rep., 2021.

[11] C. I. Calle, "The electrostatic environments of mars and the moon," in *Journal of Physics: Conference Series*, vol. 301, no. 1. IOP Publishing, 2011, p. 012006.

[12] J.-P. Williams, D. Paige, B. Greenhagen, and E. Sefton-Nash, "The global surface temperatures of the Moon as measured by the diviner lunar radiometer experiment," *Icarus*, vol. 283, pp. 300–325, 2017.

[13] D. B. J. Bussey, P. D. Spudis, and M. S. Robinson, "Illumination conditions at the lunar south pole," *Geophysical Research Letters*, vol. 26, no. 9, pp. 1187–1190, 1999.

[14] P. Gläser, J. Oberst, G. Neumann, E. Mazarico, E. Speyerer, and M. Robinson, "Illumination conditions at the lunar poles: Implications for future exploration," *Planetary and Space Science*, vol. 162, pp. 170–178, 2018.

[15] J. Fincannon, "Lunar south pole illumination: review, reassessment, and power system implications," in *Proceedings of the AIAA International Energy Conversion Engineering Conference and Exhibit*, 2007, p. 4700.

[16] B. Day and E. Law, "NASA's Moon Trek portal: New capabilities supporting mission planning and engagement," 2022.

[17] J.-P. Williams, B. Greenhagen, D. Paige, N. Schorghofer, E. Sefton-Nash, P. Hayne, P. Lucey, M. Siegler, and K. M. Aye, "Seasonal polar temperatures on the Moon," *Journal of Geophysical Research: Planets*, vol. 124, no. 10, pp. 2505–2521, 2019.

[18] J. Fincannon, "Lunar polar illumination for power analysis," in *Proceedings of the AIAA International Energy Conversion Engineering Conference*, 2008, p. 5631.

[19] LSPET (Lunar Sample Preliminary Examination Team), *Preliminary Examination of Lunar Samples*. NASA: NASA SP-235, 1970.

[20] Unity Technologies, "Unity," 2024, game development platform. [Online]. Available: https://unity.com/

[21] E. Olson, "AprilTag: A robust and flexible visual fiducial system," in *Proceedings of the IEEE International Conference on Robotics and Automation*, 2011, pp. 3400–3407.

[22] M. J. Cintala and K. M. McBride, "Block distributions on the lunar surface: A comparison between measurements obtained from surface and orbital photography," Tech. Rep., 1995.

[23] T. Krajník, M. Nitsche, J. Faigl, P. Vaněk, M. Saska, L. Přeučil, T. Duckett, and M. Mejail, "A practical multirobot localization system," *Journal of Intelligent & Robotic Systems*, vol. 76, pp. 539–562, 2014.

[24] B. Sekachev, N. Manovich, M. Zhiltsov, A. Zhavoronkov, D. Kalinin, B. Hoff, TOsmanov, D. Kruchinin, A. Zankevich, DmitriySidnev, M. Markelov, Johannes222, M. Chenuet, a andre, telenachos, A. Melnikov, J. Kim, L. Ilouz, N. Glazov, Priya4607, R. Tehrani, S. Jeong, V. Skubriev, S. Yonekura, vugia truong, zliang7, lizhming, and T. Truong, "opencv/cvat: v1.1.0," Aug. 2020. [Online]. Available: https://doi.org/10.5281/zenodo.4009388

[25] A. Kirillov, E. Mintun, N. Ravi, H. Mao, C. Rolland, L. Gustafson, T. Xiao, S. Whitehead, A. C. Berg, W.-Y. Lo *et al.*, "Segment anything," in *Proceedings of the IEEE/CVF International Conference on Computer Vision*, 2023, pp. 4015–4026.

[26] J. L. Schönberger and J.-M. Frahm, "Structure-from-Motion Revisited," in *Proceedings of the IEEE/CVF Conference on Computer Vision and Pattern Recognition*, 2016.

[27] B. Mildenhall, P. P. Srinivasan, M. Tancik, J. T. Barron, R. Ramamoorthi, and R. Ng, "NeRF: Representing scenes as neural radiance fields for view synthesis," *Communications of the ACM*, vol. 65, no. 1, pp. 99–106, 2021.

[28] M. Hansen, C. Adams, T. Fong, and D. Wettergreen, "Analyzing the effectiveness of neural radiance fields for geometric modeling of lunar terrain," in *Proceedings of the IEEE Aerospace Conference*, 2024, pp. 1–12.

BIOGRAPHY

Joseph M. Cloud *is a robotics engineer in the Advanced Engineering Development Branch at NASA's Kennedy Space Center, where he has worked since 2019. He received his honors B.S. in computer engineering from the University of Texas at Arlington in 2019 and his Ph.D. in intelligent systems and robotics in 2024. His work applies machine learning and computer vision to planetary robots, with specific interests in learning-based trajectory generation techniques, autonomous excavation, and hazard detection.*

Andrew J. Nick *received a B.S. in Mechanical Engineering from Florida Institute of Technology in 2007. He was a contractor for NASA at the Kennedy Space Center for over 13 years before converting to civil servant in 2020. As a founding member of Swamp Works at KSC, he has spent most of his career developing robotic systems for exploration and resource utilization of planetary surfaces. He is an SME in the Granular Mechanics and Regolith Operations (GMRO) laboratory.*

Bradley C. Buckles *is a robotics engineer in the Exploration Research and Technology Programs Directorate at NASA Kennedy Space Center. He is an SME in autonomous systems and robotics, focusing on robotic surface operations including excavation and construction. He currently serves as the autonomy lead for the ISRU Pilot Excavator (IPEx) project.*

Kyle L. Dixon *serves as NASA KSC's GMRO aka "Swamp Works" Laboratory Manager and the KSC Exploration & Research Technology Programs- Spaceport Technologies Office, Ground & Surface Systems Operations Subject Matter Expert. Kyle is also a Project Manager for the Universal Propellant Servicing System and the Lunar Terrain Vehicle Lunar Dust Mitigation Analysis, Design, and Test project. Kyle has over 36 years of launch processing and launch & landing operations experience. Kyle holds a B.S. in Aerospace Engineer from the Georgia Institute of Technology, is married to his wife of 36 years, Sandra, has two sons and three grandchildren.*

Thomas J. Muller *is a robotics engineer supporting the Exploration Research and Technology Programs Directorate at NASA Kennedy Space Center as a contractor at Bennett Aerospace. He is an SME in robotics systems focusing on communications and embedded systems. He received a B.S. in Computer Engineering at Florida Tech in 2022.*

Victoria V. Ortega *received a B.S. in Mechanical Engineering from Carnegie Mellon University in 2022. She worked in Swamp Works at NASA Kennedy Space as a co-op in 2021 and started her full-time career in 2022. Since then, she has assumed roles as a lead design and test engineer while supporting ISRU Pilot Excavator and other projects.*

Jonathan "Drew" Smith *is a robotics engineer, Principal Investigator, and a founder of Swamp Works at Kennedy Space Center. He joined NASA in 2009 after earning a B.S. in Mechanical Engineering from the University of North Florida. He is a subject matter expert in off-Earth excavation and has designed and tested multiple percussive excavation end effectors for NASA's Jet Propulsion Laboratory, Glenn Research Center, and Johnson Space Center. He is also an inventor of patented extraterrestrial mining robots for in-situ resource utilization. Drew is currently the Lead Design Engineer for Swamp Works.*

Casey J. Clark *received a B.S. and M.S. in Aerospace Engineering from Florida Institute of Technology in 2016 and 2018, respectively. He is the lead test engineer at Swamp Works NASA Kennedy Space Center. His interests include nonlinear control systems, multivariable feedback control systems, cryobotics and robotic design*

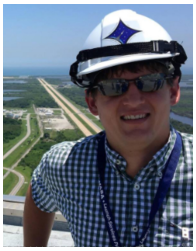

Jeffrey E. Dyas *is a systems engineer at NASA's Kennedy Space Center, where he has worked since 2016. He received a B.S. in mechanical engineering from Auburn University in 2014, M.S. in Industrial and Systems Engineering from University of Alabama in Huntsville in 2016, M.S. in Industrial and Organizational Psychology from University of Alabama in Huntsville in 2018, and M.S. in Aerospace Systems Engineering from University of Alabama in Huntsville in 2019. His research focuses on alternative methods requirement-based system design using value-based design via system level optimization of stakeholder preferences. He currently supports multiple projects at KSC as a systems engineer, including ISRU Pilot Excavator, CLPS Electrodynamic Dust Shield, and Moon 2 Mars Pre-Formulation Model-based Systems Engineering Team.*

Elizabeth L. Zhang *is a co-op intern at NASA Kennedy Space Center in Swamp Works since 2023. She completed her B.S. in Engineering Physics at the University of Illinois Urbana-Champaign in 2024 and is currently pursuing her M.S. in Mechanical Engineering at Carnegie Mellon University.*

Kurt W. Leucht *received a B.S. in Electrical Engineering from Missouri University of Science and Technology in 1994 and an M.S. in Space Systems from Florida Tech in 1998. He has been with NASA's Kennedy Space Center for 34 years, working in electronic hardware analysis and software development & testing groups. For the last decade, he has worked in the NASA Swamp Works in-situ resource utilization group, helping develop robotic systems to support future crewed Artemis lunar missions.*

Robert P. Mueller *is a Senior Technologist for Advanced Projects Development at NASA Kennedy Space Center (KSC) in the Exploration Research and Technology Programs Directorate. He is the co-founder of the NASA Swamp Works innovation labs and the KSC Granular Mechanics & Regolith Operations (GMRO) Lab. Technical expertise includes Robotics, Mechanical Systems Design, Composite Materials, In-Situ Resource Utilization (ISRU), Planetary Outpost Construction, Surface & Ground Operations, Conceptual Systems Design and Mission Architecture Design.*

Jason M. Schuler *is a mechanical engineer and founding member of Swamp Works - a team at Kennedy Space Center devoted to developing robotic technologies to use space resources. He is a co-inventor of RASSOR - aka Regolith Advanced Surface Systems Operation Robot and has spent the last 16 years developing technologies that will interact with extra-terrestrial regolith. Jason is currently the Principal Investigator for the ISRU Pilot Excavator project to develop a robotic system to demonstrate large scale lunar regolith excavation on the Moon.*